SLAC – PUB – 3880
February 1986
(E/I)

THE NEW DRIFT CHAMBER FOR THE MARK II DETECTOR AT THE SLAC LINEAR COLLIDER*

GAIL G. HANSON

Stanford Linear Accelerator Center, Stanford University,

Stanford, California 94305, U.S.A.

A new central drift chamber has been constructed for the Mark II detector for use at the new SLAC Linear Collider. The design of the new chamber is based on a multi-sense-wire cell of the jet–chamber type. In addition to drift–time measurements, pulse–height measurements from the sense wires provide electron–hadron separation by dE/dx. The chamber has been installed in the detector and is being tested at PEP before being moved to the SLC. The design and construction of the chamber, as well as initial performance results from the PEP data, are presented.

Presented at the Wire Chamber Conference, Vienna, Austria,
February 25-28, 1986

* Work supported by the Department of Energy, contract DE – AC03 – 76SF00515.

1. Introduction

The Mark II detector [1], which has run successfully at both the SPEAR and PEP e^+e^- storage rings at SLAC, has been upgraded for use as the first detector at the new SLAC Linear Collider (SLC) [2]. Studies of Z^0 physics are expected to begin at the SLC in January, 1987. The detector is being brought into operation at PEP before being moved to the SLC so that both the hardware and software are ready for data taking as soon as the SLC turns on.

The new drift chamber forms the heart of the Mark II detector for the SLC [3], shown in fig. 1. We describe here briefly the components of the detector. The drift chamber is cylindrical and is supported inside a 4.5 kG conventional solenoidal magnet. The magnet flux return iron is unchanged from the old detector and so limits the outer radius of the drift chamber. The magnet coil has been replaced with a new one of design similar to the previous one. Between the coil and the drift chamber are new scintillation counters used in the trigger and to measure time of flight. The lead and liquid argon electromagnetic calorimeter surrounding the coil is unchanged from the previous detector. New endcap gas electromagnetic calorimeters cover most of the region between the liquid argon calorimeter and the beam line. The muon identification system is unchanged. At the SLC there will also be high–resolution vertex detection and a small–angle luminosity monitor which cannot be tested at PEP.

2. Drift Chamber Design

Our primary goal in designing the new drift chamber was compatibility with the physics we expect to do at the Z^0. The general considerations were:

a) Good momentum resolution in the existing 4.5 kG field;

b) Good solid angle coverage;

c) Ease of pattern recognition and high tracking efficiency at the Z^0;

d) dE/dx as an independent aid to calorimetry for electron–hadron separation for momenta less than about 10 GeV/c.

2.1 Cell Design

The design of the drift chamber is based on a multi–sense–wire cell, shown in fig. 2, which is a shortened version of the jet–chamber configuration [4]. The cell contains six sense wires staggered ± 380 μm from the cell axis to provide local left–right ambiguity resolution. The spacing between sense wires, 8.33 mm, was chosen to be as small as we thought was practical in order to obtain a small double–track separation, which is approximately half the sense wire spacing. The half–width of the cell, 3.3 cm in the center, was constrained by the effect of diffusion for a gas at atmospheric pressure. There are two guard wires on either end of the cell for shaping the electric field and equalizing the gains of the sense wires. Potential wires are placed between the sense wires to control the gain of the sense wires separately from the drift electric field, reduce the signal coupling between adjacent sense wires, and reduce the electrostatic deflection of the staggered sense wires. The signal coupling between adjacent sense wires is about 7% . (It would be 17% without the potential wires.) The electrostatic deflection of the sense wires is about 60 μm as we operate it, with a small charge on the potential wires.

The cell design allows us to achieve a very uniform electric drift field which gives a nearly linear time–distance relation over most of the cell. At the pattern

recognition stage, track segments are found in each cell and then linked to form tracks. The local left-right ambiguity resolution and the linear time–distance relation make pattern recognition much easier.

The sense wires are 30 μm gold–plated tungsten, tensioned to 113 gm to give a 90 μm gravitational sag. The potential and guard wires are 102 μm gold–plated Inconel 600, tensioned to have the same gravitational sag as the sense wires. There are nineteen field wires in each cell with 4.16 mm spacing. They are made of 178 μm gold–plated beryllium–copper. The end field wire has a larger diameter (305 μm) in order to keep the field below about 20 kV/cm on the surface of the wire to prevent whisker growth.

2.2. Chamber Design

The drift chamber consists of twelve concentric cylindrical layers of cells. Alternate layers have their wires parallel to the cylinder axis or at $\sim \pm 3.8°$ to the cylinder axis to provide stereo information. (The stereo angle is achieved by stringing the wires with an offset of five half-cells between the two ends.) The angular offsets between the starting points of the cell patterns in the axial layers were adjusted to maximize the distance between tracks and the sense and field wire positions. The radial distance between layers is maintained at 2.5 cm minimum, including the displacement of stereo wires toward smaller radius in the center of the chamber, in order to control the change in gain along the length of the chamber as cells in adjacent stereo and axial layers change their relative orientation. The active length of the chamber is 2.30 m. The overall chamber layout is shown in fig. 3 and the design parameters are given in Table I. There are a total of 5832 sense wires and 72 measurements of drift time and dE/dx

for tracks traversing the full radial extent of the chamber. The total number of wires is 36,936.

2.3. Mechanical Design

The wires were strung between 2–inch–thick aluminum endplates. The wires pass through slots in the endplates for each row of nineteen wires in a cell. The endplates are held apart by a 2–mm–thick beryllium inner cylinder and by a 1/2–inch thick cylindrical aluminum outer shell. The total load from the wire tension is 20,000 kg. The inner radius of the drift chamber is 19.2 cm and the outer radius is 151.9 cm. The outer shell has eight large windows for access; the windows are closed with 1/4-inch aluminum panels. The inner and outer cylinders are welded to the endplates. The endplates were prestrained with 108 evenly–spaced steel tie–rods tensioned with die springs to keep the wire tension uniform; the tie–rods were removed as the wire stringing progressed.

All the wires in one row of a cell are positioned by a one–piece injection–molded Delrin 500AF feedthrough [5] which is sealed into a slot in the endplate. Each feedthrough is located on the endplate by pinning to three accurately–machined holes in both the feedthrough and the endplate. The wires are located in machined notches along one side of a central slot in the feedthrough, tensioned, and soldered to a printed circuit board epoxied to the Delrin feedthrough. For added holding strength, the ends of the wires were then epoxied to a strip of kapton which is epoxied over the printed circuit board. The inside of the slot in the aluminum is insulated with an injection–molded polysulfone sleeve. The open slot in the feedthrough permitted the wires to be strung in groups of nineteen, which saved time in the stringing; we were able to string 300 wires in an eight-hour

shift. The slot also allows access for repairs and provides for visual inspection of the interior. The gas seal over the slot is provided by a layer of silicone or SARAN® sealed to the feedthrough body with Dow Corning SILASTIC® 738 RTV and a Lexan cover. Electrical connections to the wires are made through the printed circuit board.

The primary consideration in the design of the endplate and feedthrough was accuracy in wire positioning; the expected error was ± 35 μm. Sources of errors in wire location are the following: feedthrough accuracy in machining and placement – 15 μm, error in endplate machining and placement – 25 μm, and error in wire sag and electrostatic deflection – 10 μm.

2.4. High Voltage

The drift electric field is determined primarily by the voltages on the field wires. The voltage on the potential wires determines the gain of the sense wires. The voltage on the guard wires helps to control the uniformity of gain of the six sense wires. The inner and outer cylinders are lined with copper-clad kapton to which high voltage is applied to maintain a uniform electric field in the inner and outer drift chamber layers.

A graded high voltage is supplied to each cell through a resistor–divider chain. The voltage must be graded to provide a uniform drift field over the varying width of the cell. The nineteen field wires in each cell are ganged to form nine sets of wires, each of which is at the same voltage. One high voltage power supply supplies field–wire voltage to an entire layer. The current drawn by the chamber is monitored by measuring the difference between the current drawn by the resistor chain for a known voltage drop and the current drawn from the

supply. The voltage on a field wire in the center of a cell is typically –4.5 kV at our present operating point. The potential wire and guard wire voltages are typically –1.5 kV and –200 V, respectively. The copper skins lining the inner and outer cylinders are typically at ~ -2.5 kV. The drift chamber high voltages and currents are controlled and monitored using an IBM PC/AT computer.

3. Drift Chamber Electronics

A block diagram of the drift chamber electronics is shown in fig. 4. The preamplifiers are mounted directly on the feedthroughs. A large aluminum rf shield covers the entire endplate. The postamplifiers are located in crates mounted near the drift chamber on the magnet iron. The drift times and pulse heights are measured by FASTBUS modules in the electronics house. Data is read out through Scanner Processor modules and a FASTBUS Interface by a VAX 8600 computer. More information on the data acquisition can be found in Reference 6.

3.1. Preamplifiers

The preamplifier is a voltage amplifier based on the Plessey SL560C chip. There are six channels per board, corresponding to the six sense wires in a drift chamber cell. The voltage gain is 25. The input noise is 15.5 μV rms. The risetime is 9 ns. The preamplifier contains crosstalk canceling resistors to reduce the crosstalk between adjacent sense wires and next-to-adjacent sense wires to the level of less than 1.5% . They feed an attenuated negative signal from a sense wire to cancel the positive signal from the drift chamber crosstalk. The linearity is $\pm 6\%$ for input signals of 0.5 to 20 mV. The power dissipation is 83 mW per

channel. A calibration signal is fanned out to each channel on the preamplifier board.

3.2. Postamplifier

The postamplifier further amplifies the drift chamber pulse, shapes the pulse, splits the pulse for timing and dE/dx measurement, and discriminates the pulse for the timing channel. Careful pulse shaping is needed to obtain optimal double track resolution. Some of the specifications are listed here:

a) A two–stage pole-zero filter cancels the $1/t$ tail.

b) The gain is 100 for the timing channel and variable in steps from 1.1 to 16.4 for the dE/dx channel. In reality, the gain is dependent on the shaping of the pulse.

c) The discriminator is a LeCroy MVL407 comparator with output pulse width given by time over threshold.

d) The calibration pulse is fanned out to the preamplifiers.

e) There is separate cable compensation for the timing and dE/dx channels.

More details on the preamplifier and postamplifier can be obtained from Reference 7.

3.3. Time Digitization

Drift times are digitized by LeCroy 1879 TDC's, which are newly–developed FASTBUS modules based on a silicon-on-sapphire shift register. There are 96 channels per module. The nominal bin width is 2 ns, although the clock speed can be modified. The measured time resolution is less than 1 ns, with channel-to-channel correlation less than 0.4 ns^2. Multiple hits are recorded for each wire.

3.4. dE/dx Electronics

For dE/dx measurements drift chamber pulses are digitized using 100-Mhz 6–bit Flash ADC's. The digitization is performed using a 6-bit TRW 1029J7C converter. The 16-channel FASTBUS dE/dx modules were designed at SLAC and are described in detail in Reference 8. One-third of the drift chamber has been instrumented for data taking at PEP. The rest of the system is in production and will be operational at the SLC by January, 1987.

3.5. Scanner Processor

The readout of the FASTBUS modules, the TDC's and Flash ADC's, is controlled by a general-purpose programmable FASTBUS module, the SLAC Scanner Processor (SSP) [9]. On the crate level, SSP's provide control, buffering, and preprocessing of the data. Preprocessing includes sparse scan and pedestal and gain corrections. The readout of all crate SSP's on a single FASTBUS cable segment is controlled by a system SSP.

4. Drift Chamber Operation and Performance

4.1. Drift Chamber Operation

The drift chamber was put into operation with the full complement of timing electronics in July, 1985. Data was taken with cosmic rays. Channel-to-channel timing differences are measured using calibration pulses and corrected for in the SSP's. Much information about chamber performance can be obtained from the distribution of time differences for the staggered sense wires in individual cells. For any triplet of adjacent staggered sense wires the quantity $(t_1 + t_3)/2 - t_2$, where t_i are the drift times for the three wires in the triplet, shows a double

peak due to tracks passing on either side of the sense wire plane. The distance between the peaks is twice the stagger between the sense wires divided by the drift velocity. The single-wire position resolution can be found from the width of the peak. In order to make use of information from all six sense wires in a cell in a single plot, we examine the quantity $((t_1 + t_3 - 2t_2) - (t_4 + t_6 - 2t_5))/8$, where the t_i are the drift times from the six sense wires in the cell. A distribution of this quantity is shown in fig. 5. From such distributions we can measure the intrinsic position resolution as a function of drift time and also monitor the drift velocity, v_D. The intrinsic resolution is not affected by the overall timing constant relating the TDC stop to the trigger time, t_0, or by geometric constants relating wires in one cell to wires in the other cells.

Guided by previous work with prototypes, we established an operating point in the gas 89% argon/10% CO_2/1% methane (HRS gas) by measuring the intrinsic resolution at various gas gains and threshold settings. First we chose the lowest threshold for practical running, which was governed by noise in the electronics. Then we chose the lowest gain for which the intrinsic position resolution was not degraded. The threshold setting corresponds to 80 μV at the preamp input. The gas gain is $\sim 2 \times 10^4$. The electric drift field is 900 V/cm for which variations in drift velocity as a function of drift field are minimized. The drift velocity is 52 μm/ns, and the Lorentz angle is 18.9° in the 4.5 kG magnetic field.

4.2. Position Resolution and Tracking

Our goal was to measure positions from drift times to an accuracy of 200 μm or better. The position resolution is determined principally by details of the electron drift in the gas. We expect a contribution from diffusion of about 150 μm,

depending on the drift distance. The position error due to the electronics is 50 μm in HRS gas, and the error from wire placement should be about 35 μm. For 200 μm position resolution, we predict a momentum resolution of $\sigma(p)/p^2 \leq 0.15\%$ GeV^{-1} over 70% of the solid angle using a constraint that the tracks originate at the (SLC) beam interaction point. This increases to 0.45% GeV^{-1} at $\cos\theta = 0.85$, where θ is the polar angle. Multiple scattering contributes an additional error of $\sigma(p)/p = 1.4\%$. There are at least 20 measurements per track over 90% of the solid angle. The resolutions in azimuthal and polar angle are $\sim$ 0.1 mr and $\sim$ 1.2 mr, respectively, over 70% of the solid angle using a vertex constraint.

The algorithms for track finding and fitting were developed using Monte Carlo simulations. Briefly, the drift times are converted to drift distances using a time-distance relation of the form

$t < t_{NEAR}$:

$$x = v_{NEAR}(t - t_0)$$

$t_{NEAR} < t < t_{FAR}$:

$$x = v_{NEAR}(t_{NEAR} - t_0) + v_D(t - t_{NEAR}) \tag{1}$$

$t > t_{FAR}$:

$$x = v_{NEAR}(t_{NEAR} - t_0) + v_D(t - t_{NEAR})$$

$$+ a_{FAR}(t - t_{FAR})^2 \ .$$

As stated previously, the time-distance relation is linear over most of the cell. Track segments are found in each axial cell and linked in curvature and azimuth to form tracks. Stereo segments are then picked up. After all the drift chamber

hits associated with a track are found, a full track fit is done. The tracking algorithms worked very well initially; cosmic ray tracks were found the day after the drift chamber was put into operation.

We began to take e^+e^- colliding beam data at PEP in November, 1985. Using clean events from Bhabha scattering ($e^+e^- \rightarrow e^+e^-$), we have begun to determine constants for the track fitting. Using the design values for the wire positions and varying only t_0, the drift velocity, and the Lorentz angle, we met our design goal of 200 μm single-wire position resolution. By using the full form of the time-distance relation, including the nonlinear term, as shown in Eq. (1), and varying the constants separately for the two sides of the cell and for each of the 72 layers of wires, we obtained rms residuals vs. drift distance as shown in fig. 6. Also shown in fig. 6 is the intrinsic resolution vs. drift distance. The resolution from tracking is then as good as the intrinsic resolution, with an average of about 175 μm. We are now studying systematic errors in wire positions, time-slewing corrections using charge measurement from the Flash ADC's, and tracking efficiency and resolution for tracks at small polar angles. We are also studying complex multihadronic events, such as that shown in fig. 7, in order to improve the track-finding algorithms.

4.3. dE/dx Measurement

dE/dx information is obtained from pulse height measurement of the sense wire signals. The drift chamber provides 72 samples of 8.33 mm size, for which the calculated resolution in HRS gas is 6.9% . We have measured a dE/dx resolution of 5.7% for HRS gas using a prototype chamber in a positron test beam. The dE/dx separation between particles of different types is given by

the quantity $\Delta E/\sigma$, where ΔE is the difference in dE/dx between the particles and σ is the resolution. The separation for electrons and pions, muons, kaons, and protons as a function of particle momentum is shown in fig. 8. Since there are regions of ambiguity, time-of-flight information in conjunction with dE/dx provides considerable improvement. We calculate that the separation is better than three standard deviations for momenta up to 6 GeV/c. For 80% electron tagging efficiency a 10 to 1 pion rejection can be expected for momenta up to 12.5 GeV/c.

The 10:1 electron–hadron separation from dE/dx and time-of-flight is in addition to the electron identification already provided by the electromagnetic calorimetry. The dE/dx identification is particularly useful for particles in the centers of jets. Using the calorimeter alone the hadron rejection rate is expected to be 20:1 in the center of a jet at the Z^0 compared with 200:1 for isolated electrons. Using the dE/dx information in addition increases the rejection rate to $> 500 : 1$ even in the core of a jet. In addition, dE/dx information can be used to improve the double track resolution for tracking. Pulse height corrections for time-slewing can also improve the position resolution.

The dE/dx electronics for one–third of the chamber has just become operational. Digitized pulses on the six sense wires in a cell for two crossing tracks are shown in fig. 9. We are just beginning to study the algorithms and pulse height corrections needed for particle identification.

5. Conclusions

The new Mark II drift chamber has exceeded the design goals for position resolution; however, more work is needed to refine the track–finding algorithms.

dE/dx measurement is still at a very early stage. Data which we have taken at PEP is being used to gain experience with tracking and dE/dx measurement before we move to the SLC. We look forward to using the drift chamber to carry out a very exciting physics program at the SLC.

We would like to acknowledge the efforts of the many physicists, engineers, technicians, and others who worked on the design, prototyping, construction, installation and commissioning of the drift chamber and electronics.

References

[1] R. H. Schindler, *et al.*, Phys. Rev. D 24, 78 (1981).

[2] SLAC Linear Collider Conceptual Design Report, SLAC–229, June, 1980.

[3] Proposal for the Mark II at SLC, SLAC-PUB-3561, CALT-68-1015, April, 1983.

The collaboration for the Mark II at the SLC consists of physicists from Caltech, University of Colorado, University of Hawaii, Indiana University, Johns Hopkins University, Lawrence Berkeley Laboratory, University of Michigan, University of California at Santa Cruz, and SLAC Groups A, C, E and H.

[4] W. Farr, *et al.*, Nucl. Instr. and Meth. 156, 283 (1978).

[5] We have since found that microdischarges occur because of voids in the Delrin; a better material should have been used.

[6] A. J. Lankford and T. Glanzman, IEEE Trans. on Nucl. Sci. NS-31, No. 1, 225 (1984).

[7] D. Briggs, *et al.*, IEEE Trans. on Nucl. Sci. NS-32, No. 1, 653 (1985).

[8] D. Bernstein, *et al.*, Proceedings of the Nuclear Science Symposium, San Francisco, CA, October, 1985, SLAC-PUB-3806.

[9] H. Brafman, *et al.*, IEEE Trans. on Nucl. Sci. NS-32, No. 1, 336 (1985).

TABLE I. Drift Chamber Parameters

Layer	Radius at Center (cm)	Stereo Angle ($degrees$)		Number of cells
		Wire 1	Wire 6	
1	27.05	0	0	26
2	38.25	3.65	4.07	36
3	48.45	0	0	46
4	59.25	-3.73	-4.00	56
5	69.45	0	0	66
6	80.15	3.76	3.96	76
7	90.35	0	0	86
8	100.95	-3.77	-3.93	96
9	111.15	0	0	106
10	121.65	3.77	3.91	116
11	131.85	0	0	126
12	142.35	-3.78	-3.89	136

Figure Captions

Fig. 1. Plan view of the Mark II detector for the SLC.

Fig. 2. Drift chamber cell structure.

Fig. 3. Overall layout of the drift chamber.

Fig. 4. Block diagram of drift chamber electronics.

Fig. 5. Drift time difference for staggered wires in a cell.

Fig. 6. Intrinsic resolution (open circles) and tracking resolution ($\times$'s) for Bhabha events.

Fig. 7. Drift chamber tracks in a multihadronic event. The short lines represent the six hit sense wires in a cell.

Fig. 8. dE/dx identification for electrons as a function of momentum.

Fig. 9. Flash ADC data showing two crossing tracks in a cell.

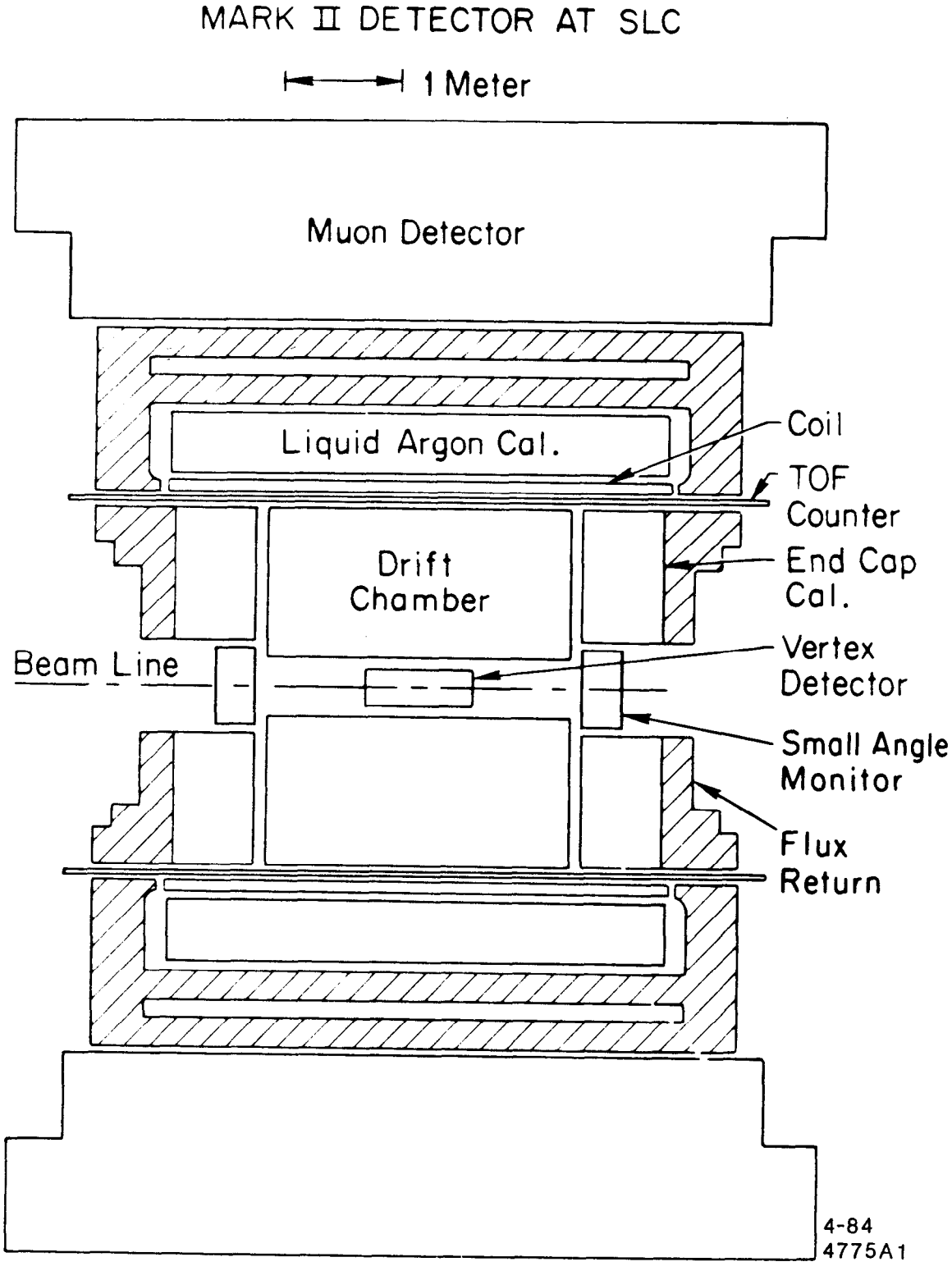
MARK II DETECTOR AT SLC
1 Meter
Muon Detector
Liquid Argon Cal.
Coil
TOF Counter
Drift Chamber
End Cap Cal.
Beam Line
Vertex Detector
Small Angle Monitor
Flux Return
4-84
4775A1

Fig. 1

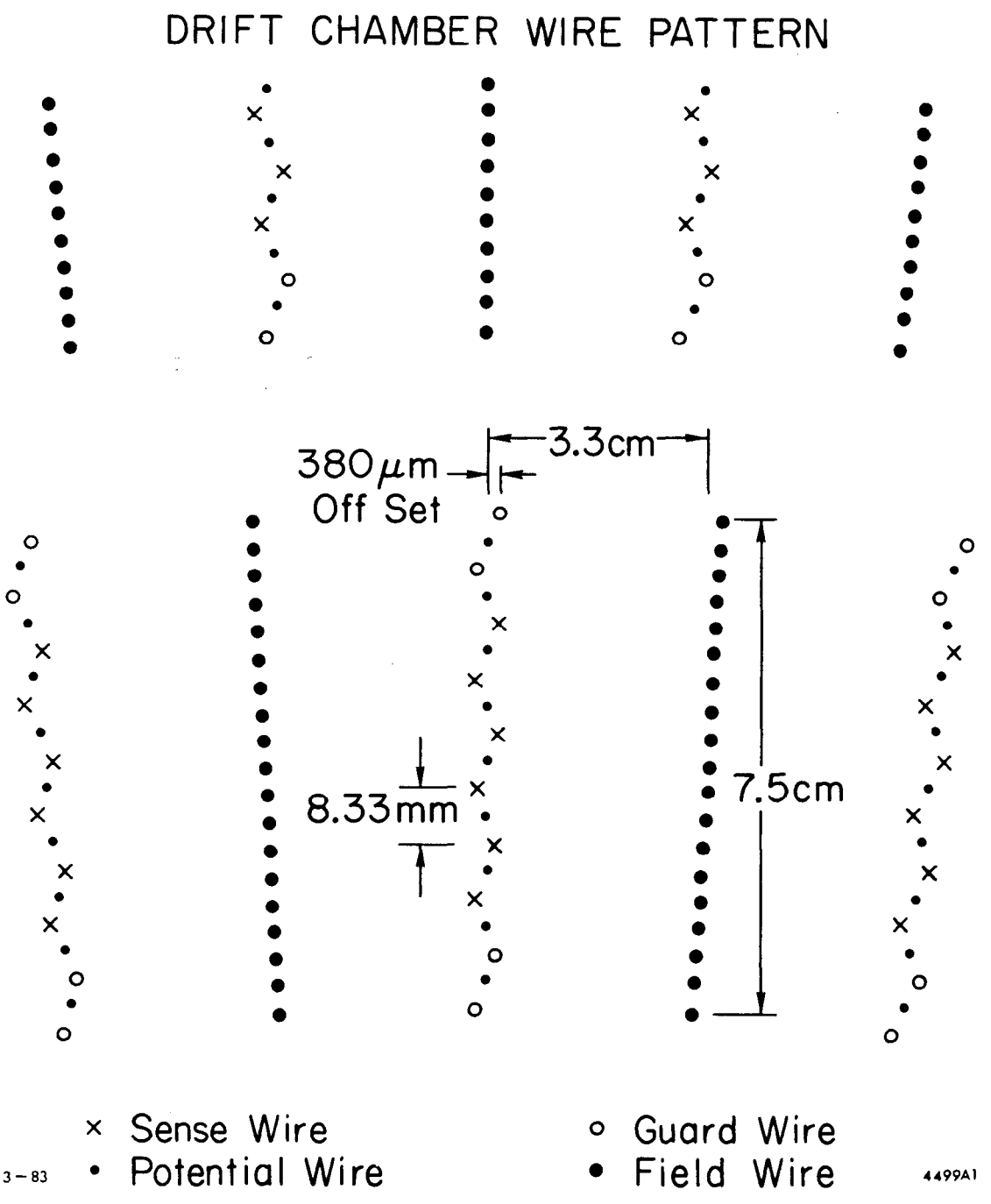
DRIFT CHAMBER WIRE PATTERN
380μm
Off Set
3.3cm
8.33mm
7.5cm
× Sense Wire
• Potential Wire
o Guard Wire
• Field Wire
3-83
4499A1

Fig. 2

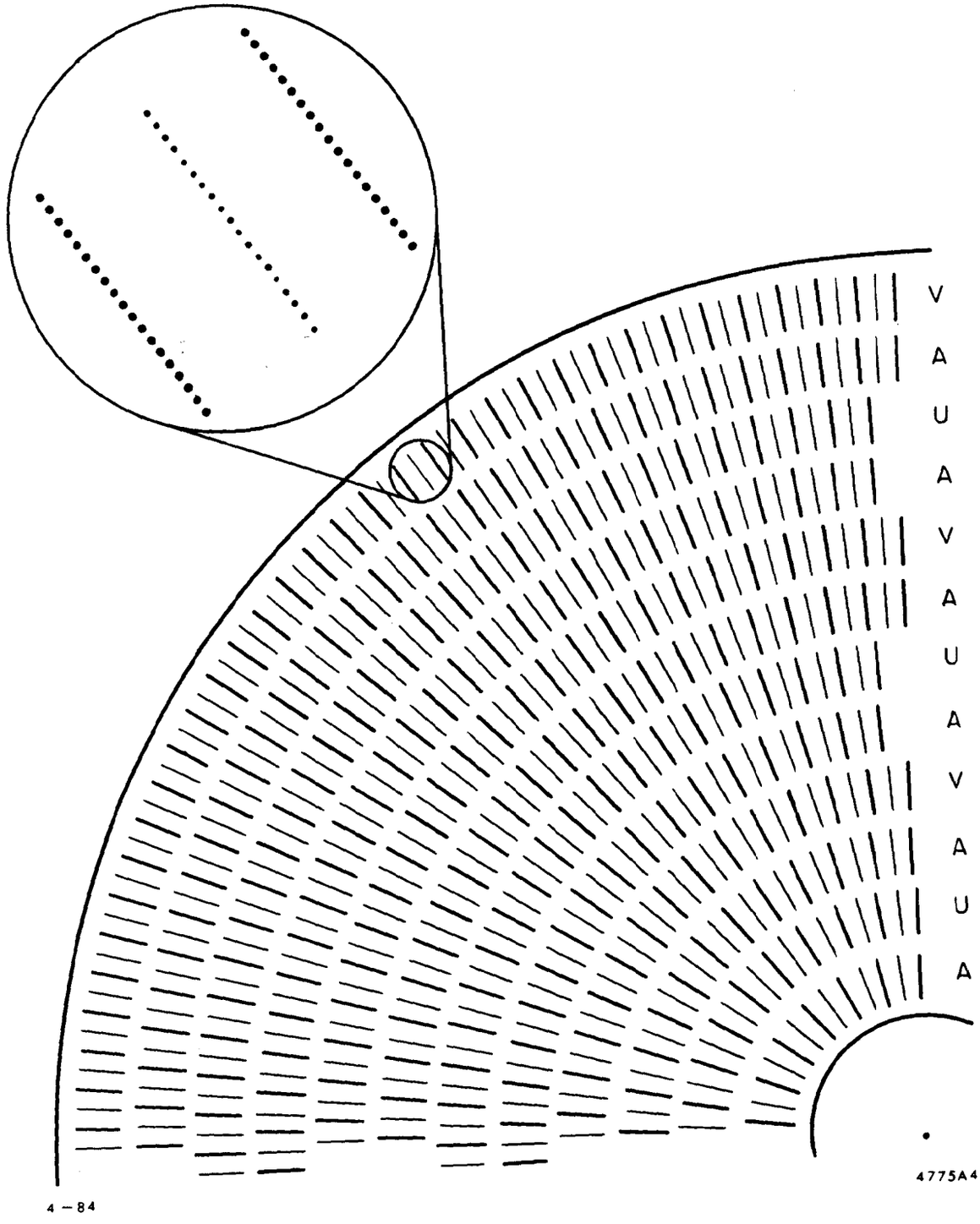

Fig. 3

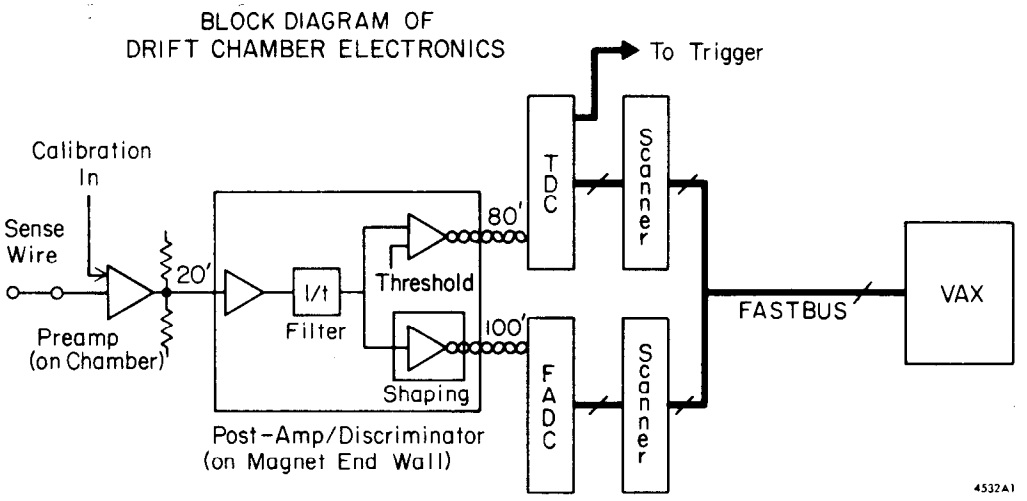
BLOCK DIAGRAM OF
DRIFT CHAMBER ELECTRONICS
To Trigger
Calibration
In
Sense
Wire
20'
Preamp
(on Chamber)
I/t
Filter
Threshold
Shaping
80'
100'
Post-Amp/Discriminator
(on Magnet End Wall)
TDC
FADC
Scanner
Scanner
FASTBUS
VAX
2-86
4532A1

Fig. 4

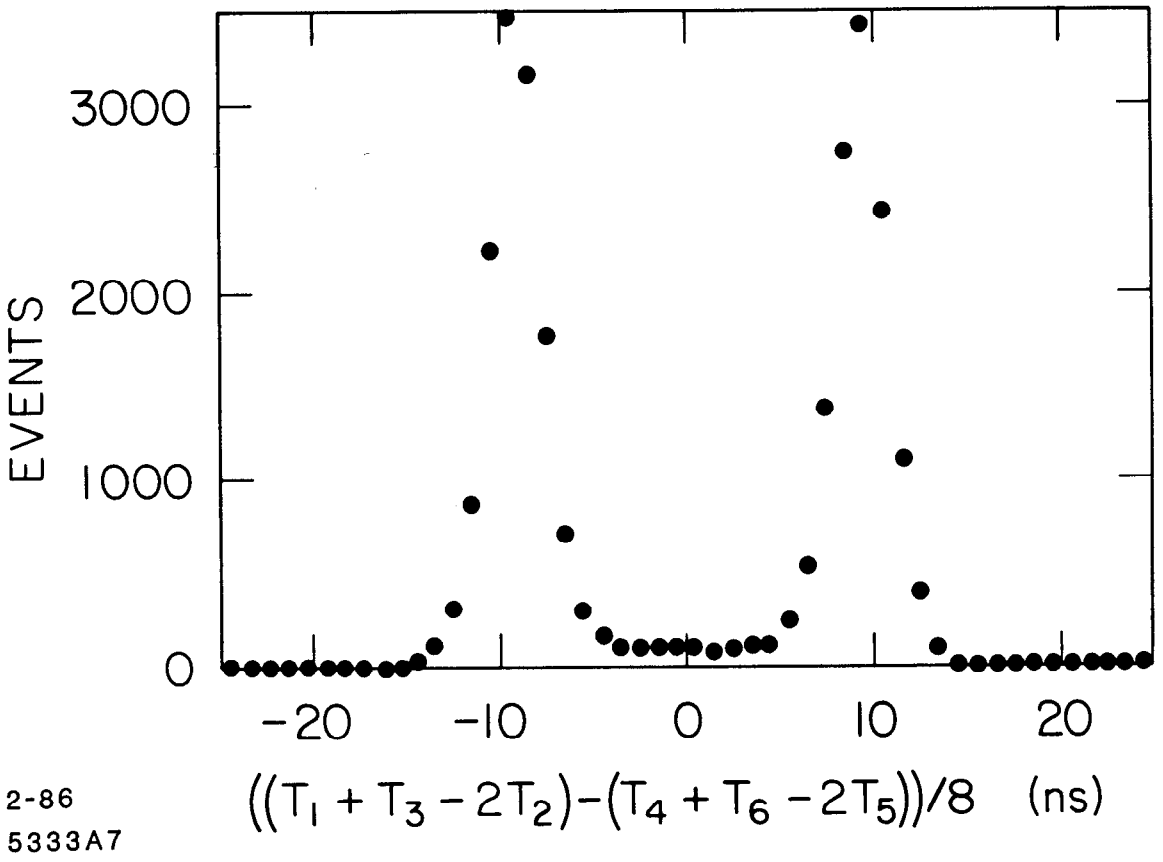
3000
2000
1000
0
EVENTS
-20
-10
0
10
20
((T1 + T3 - 2T2)-(T4 + T6 - 2T5))/8 (ns)
2-86
5333A7

Fig. 5

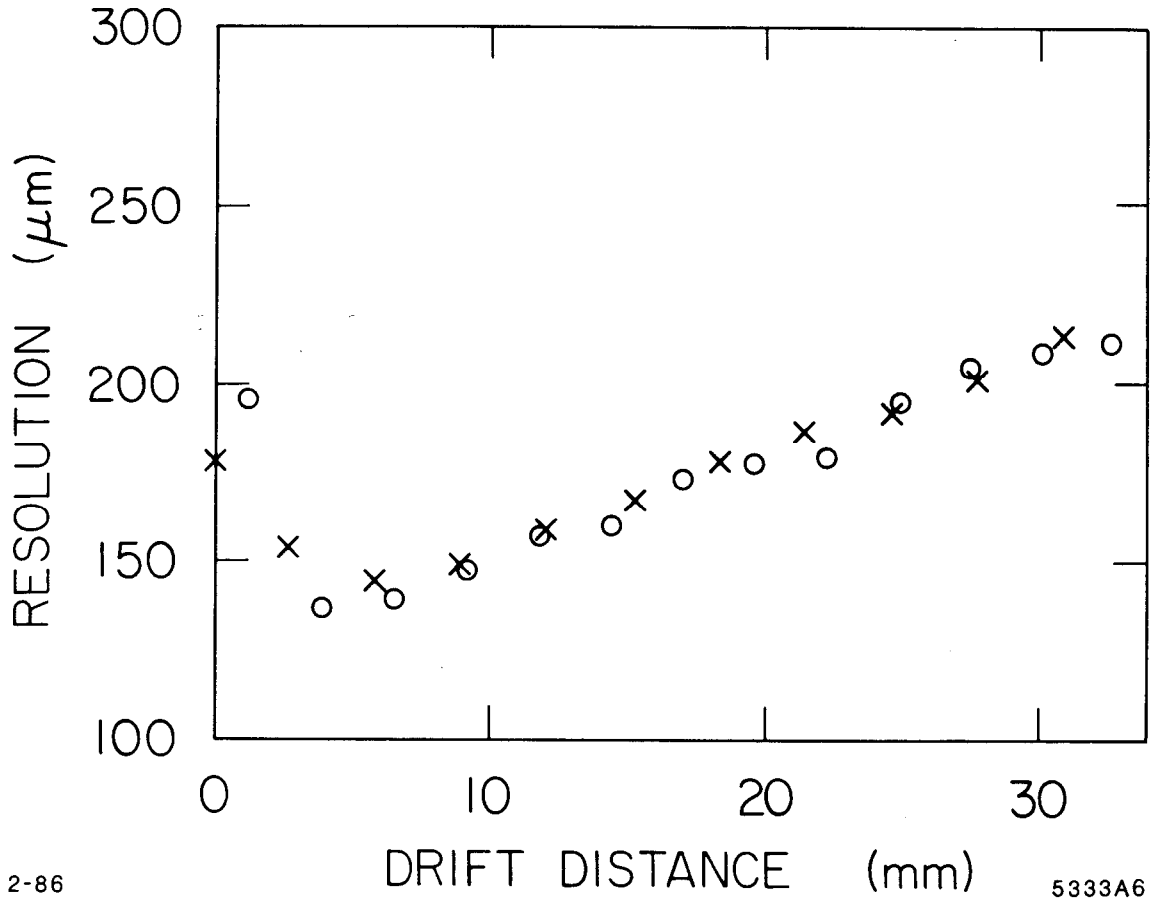
300
250
200
150
100
RESOLUTION (μm)
0
10
20
30
DRIFT DISTANCE (mm)
2-86
5333A6

Fig. 6

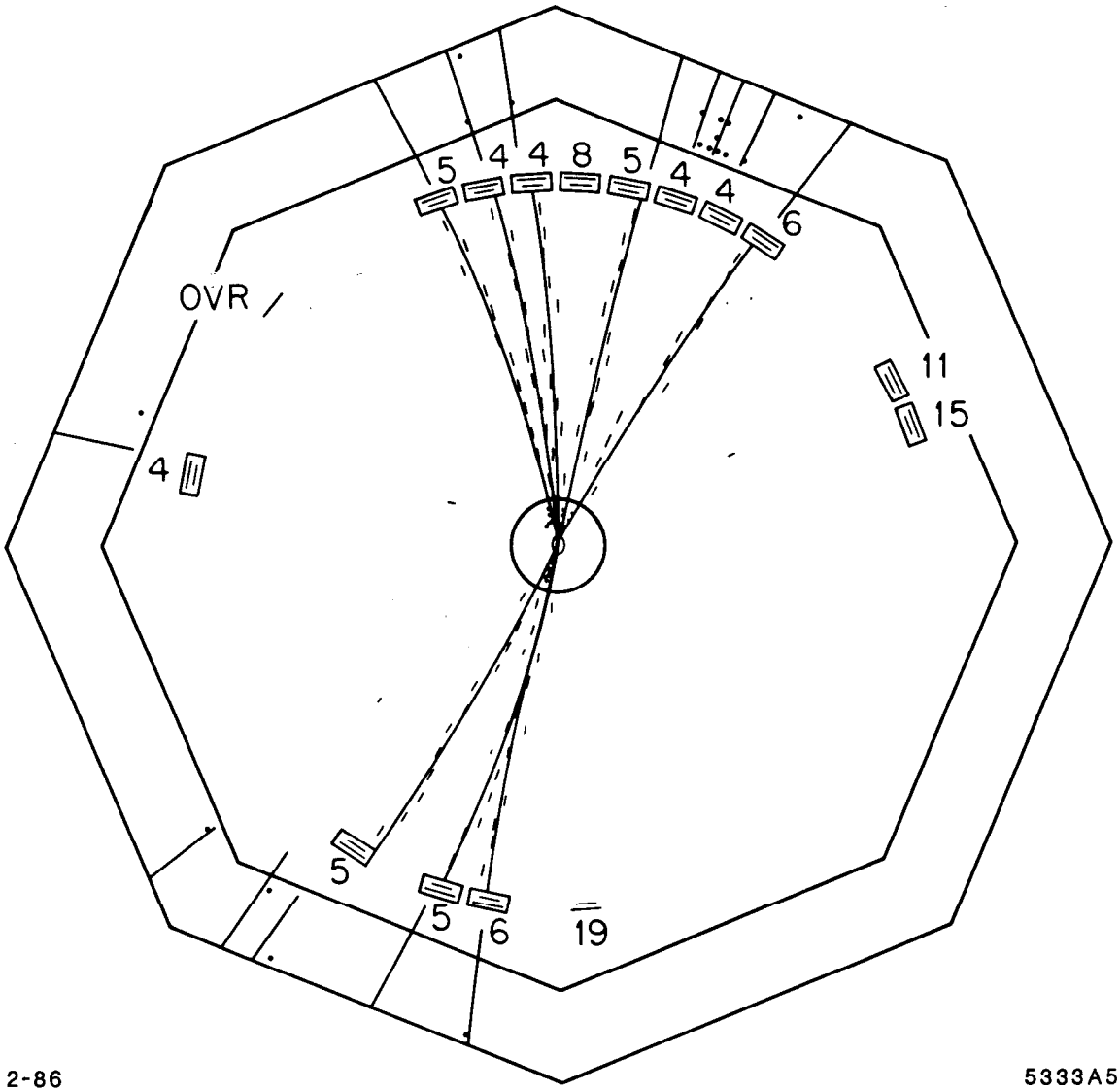

2-86

5333A5

Fig. 7

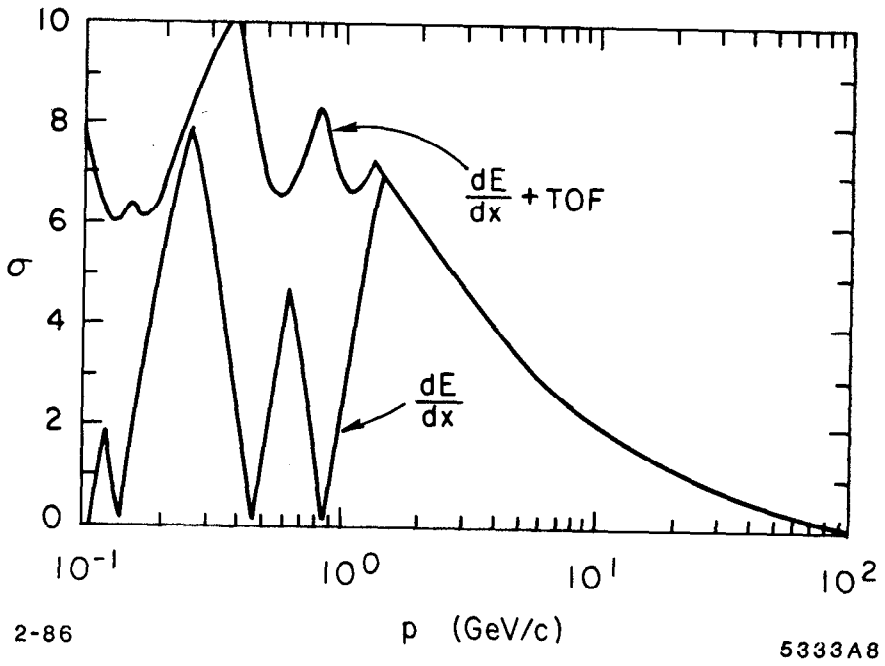

Fig. 8

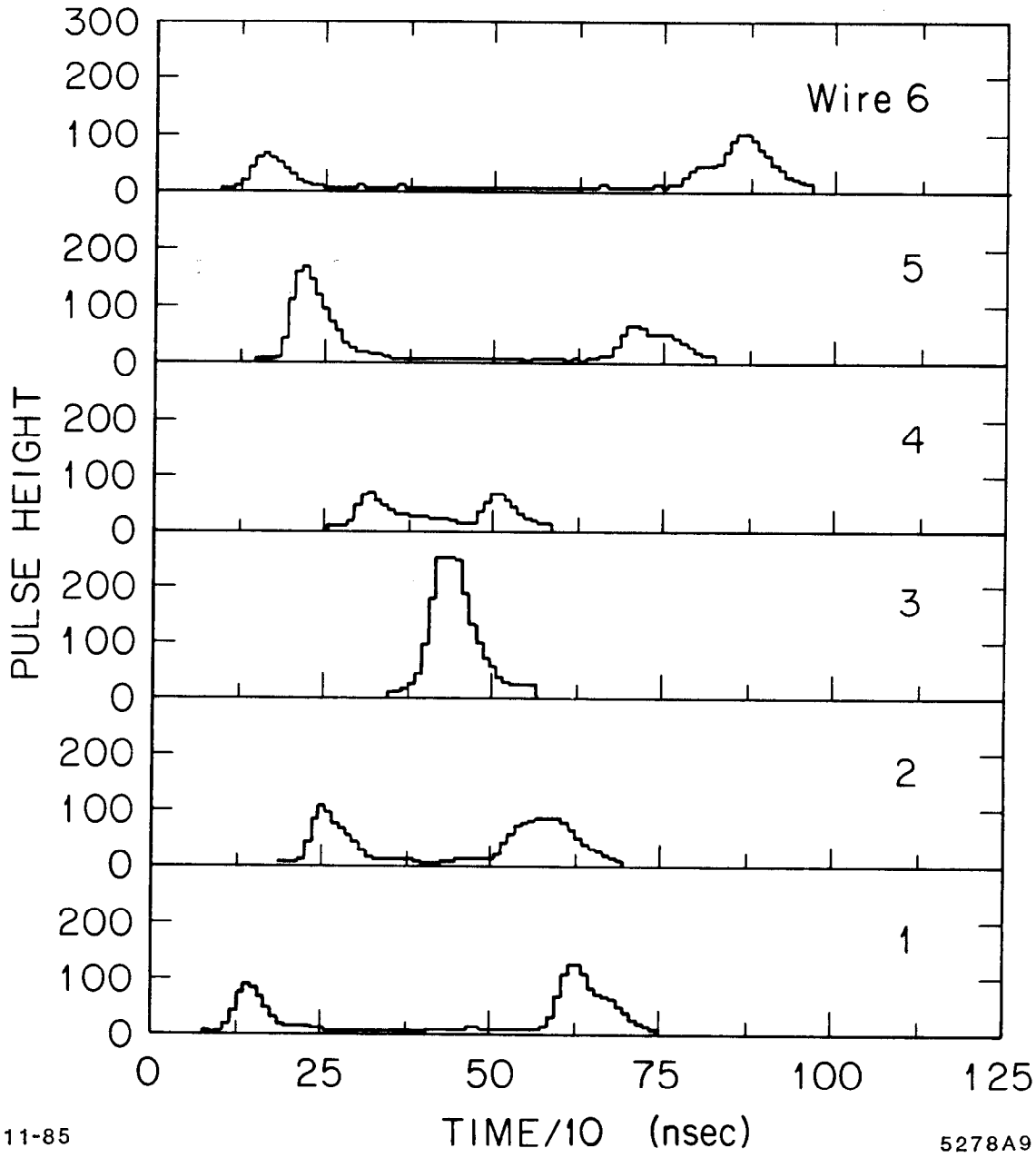
300
200
100
0
Wire 6
200
100
0
5
200
100
0
4
200
100
0
3
200
100
0
2
200
100
0
1
PULSE HEIGHT
0
25
50
75
100
125
TIME/10 (nsec)
11-85
5278A9

Fig. 9